Third-order nonlinear optical properties of dendritic molecular aggregates: Effects of fractal architecture

ARTICLE *in* INTERNATIONAL JOURNAL OF QUANTUM CHEMISTRY · SEPTEMBER 2001

Impact Factor: 1.43 · DOI: 10.1002/qua.1420

5 AUTHORS, INCLUDING:

Masayoshi Nakano
Osaka University
337 PUBLICATIONS **4,793** CITATIONS

SEE PROFILE

Third-Order Nonlinear Optical Properties of Dendritic Molecular Aggregates: Effects of Fractal Architecture

M. NAKANO, H. FUJITA, M. TAKAHATA, S. KIRIBAYASHI, K. YAMAGUCHI

Department of Chemistry, Graduate School of Science, Osaka University, Osaka 560-0043, Japan

Received 7 June 2000; accepted 12 March 2001

ABSTRACT: We investigate the microscopic third-order nonlinear optical properties, i.e., the second hyperpolarizabilities (γ), of two different sizes of molecular aggregates with a dendritic, i.e., Bethe-lattice, structure. One possesses a nonfractal structure, while the other has a fractal structure. The aggregate is treated in a two-exciton model composed of two-state monomers coupled to each other by the dipole–dipole interaction. The off-resonant γ of the aggregates are calculated by the numerical Liouville approach, including relaxation effects. The total γ value is partitioned into the contribution of virtual exciton generation, and its spatial contribution to γ is analyzed in relation to the virtual excitation processes in the perturbation theory. It is found that the intermolecular-interaction effect enhances both one- and two-exciton-generation contributions, while the relaxation effect reduces those, although the one- and two-exciton-generation contributions have mutually opposite signs. From the comparison of spatial contributions to γ between the nonfractal and fractal aggregates, an enhancement of the contribution to γ from the periphery to the core is observed in the fractal structure, while such a feature is not observed in the nonfractal structure.
 Int J Quantum Chem 84: 649–659, 2001

Key words: dendrimer; nonlinear optics; exciton; aggregate; fractal

Correspondence to: M. Nakano; e-mail: mnaka@chem.sci.osaka-u.ac.jp.

Contract grant sponsor: Ministry of Education, Science, Sports, and Culture, Japan.

Contract grant numbers: Grant-in-Aid for Scientific Research on Priority Areas 10185101, 12042248, 12740320.

Introduction

A large molecular antenna with an ordered geometry and ordered energetics has attracted much attention because of its high light-harvesting property [1–12]. It has been shown that a series of dendrimeric structures composed of phenyl rings and acetylene units exhibit a symmetric and ordered exciton funnel with a well-directed energy gradient. Dendritic molecules are characterized by a large number of terminal groups originating in a focal point (core) with at least one branch at each repeat unit. The efficient excitation energy cascading to the core is assumed to be caused by the fact that the molecular architecture provides an energy gradient as the energy decreases as a function of position from the periphery to the core and has relaxation in the exciton states [13]. Judging from these results, the features of the energy gradient and the relaxation are expected to strongly depend on the molecular architecture, the molecular size, and the unit molecular species. In our previous paper [14], we elucidated that some dendritic molecular aggregates also exhibit similar ordered energy states and directional energy transfer. However, there have been a few studies on the response properties, e.g., nonlinear optical (NLO) processes, for such systems, although the first-order optical processes, i.e., absorption and emission of light, have been investigated actively. In this study, we elucidate the features of the second hyperpolarizability γ, which is the microscopic origin of the third-order nonlinear optical phenomena, for dendritic molecular aggregates, i.e., two different sizes of dendritic aggregates with and without fractal structures, in which the monomer (chromophore) is assumed to be a dipole unit (a two-state molecular model) arranged as modeled after the Bethe-lattice type structure [10–12]. From the comparison of the results between these two types of aggregates, the role of the fractal structure in γ is investigated.

A conventional two-exciton molecular aggregate model is constructed from chromophore dipole units coupled to each other by the dipole–dipole interaction. The exciton states and transition moments are calculated by diagonalizing the model Hamiltonian matrix. Using this aggregate-state model, the time evolution of the aggregate density matrix is calculated in a numerically exact manner, i.e., the numerical Liouville approach (NLA), including relaxation effects [15]. The nonperturbative γ values are calculated using our definition of intensity-dependent γ [15]. To better elucidate the feature of γ, we analyze the spatial contribution of the virtual exciton generation to γ by partitioning total γ values into γ_{a-b} for two bases a and b, e.g., the ground and the one-exciton states [16]. This partitioned γ_{a-b} represents the contribution of the virtual excitation process involving a and b states. By using the maps of the spatial contribution to γ, we elucidate the intermolecular interaction and the relaxation effects on the spatial contribution of one- and two-exciton generations to γ. Also, we elucidate the role of the fractal structure in γ of these dendritic systems by comparing the intermolecular interaction effects on spatial contributions to γ of fractal dendritic systems with those of nonfractal dendritic systems.

Methodology

CONSTRUCTION OF A STATE MODEL FOR A MOLECULAR AGGREGATE

We consider two different sizes of dendritic molecular aggregates (Fig. 1), referred to as *D*9 and *D*24, respectively, composed of two-state monomers (chromophores). The monomer is approximated to be a dipole composed of a two-state model, and is illustrated by an arrow. The kth monomer possesses a transition energy $E_{21}^k (\equiv E_2^k - E_1^k)$ and a transition moment μ_{12}^k. This approximation is considered to be acceptable if the intermolecular distance (R_{kl}) is larger than the size of a monomer. The angle between a dipole k and a line drawn from the dipole site k to l is θ_{k_l}. The Hamiltonian for the aggregate model (composed of N monomers) is written by

$$\begin{aligned} H_{\mathrm{agg}} &= H_0 + H_{\mathrm{int}} \\ &= \sum_k^N \sum_{i_k}^2 E_{i_k}^k a_{i_k}^+ a_{i_k} + \frac{1}{4\pi\varepsilon_0} \sum_{k<l}^N \sum_{\substack{i_k i'_k \\ i_l i'_l}}^2 \mu_{i_k i'_k}^k \mu_{i_l i'_l}^l \\ &\quad \times \left[\left(\cos(\theta_{k_j} - \theta_{l_k}) - 3\cos\theta_{k_j}\cos\theta_{l_k} \right) / R_{kl}^3 \right] \\ &\quad \times a_{i_k}^+ a_{i'_k} a_{i_l}^+ a_{i'_l} \end{aligned} \tag{1}$$

where the first (H_0) and the second (H_{int}) terms on the right-hand side represent a noninteracting Hamiltonian and the dipole–dipole interaction. $E_{i_k}^k$ is an energy of the state i_k for monomer k, and $\mu_{i_k i'_k}^k$ is a magnitude of a transition matrix element between states i_k and i'_k for monomer k. The $a_{i_k}^+$ and $a_{i'_k}$ represent, respectively, the creation and annihilation operators for the i_k state of monomer k.

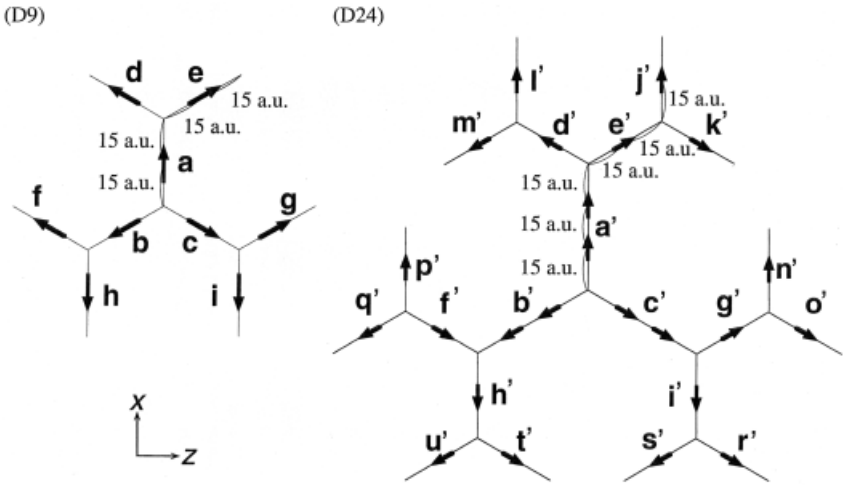

FIGURE 1. Structure and a labeling of the linear legs of two sizes of dendritic molecular aggregates [*D*9 (with a nonfractal structure) and *D*24 (with a fractal structure)] which mimic a skeleton of phenylacetylene dendrimer [10–12]. Each two-state monomer dipole unit (with transition energy $E_{21} = 38{,}000\ \text{cm}^{-1}$ and transition moment $\mu_{21} = 5$ D) is represented by an arrow. The angle between neighboring linear legs at all branching points is assumed to 120°.

By using the basis for the aggregate $\{|\varphi_{i_1}^1 \varphi_{i_2}^2 \cdots \phi_{i_N}^N\rangle\}$, which is constructed by a direct product of a state vector for each monomer $\{|\varphi_{i_k}^k\rangle\}$, the matrix elements of H_0 an is represented by

$$\langle \varphi_{j_1}^1 \cdots \varphi_{j_N}^N | H_0 | \varphi_{j_1'}^1 \cdots \varphi_{j_N'}^N \rangle = \sum_k^N E_{j_k}^k \left(\prod_{n=1}^N \delta_{j_n j_n'} \right) \quad (2)$$

and the matrix element of H_{int} is expressed by

$$\langle \varphi_{j_1}^1 \cdots \varphi_{j_k}^k \cdots \varphi_{j_l}^l \cdots \varphi_{j_N}^N | H_{\text{int}} | \varphi_{j_1'}^1 \cdots \varphi_{j_k'}^k \cdots \varphi_{j_l'}^l \cdots \varphi_{j_N'}^N \rangle = \sum_{k<l}^N \mu_{j_k j_k'}^k \mu_{j_l j_l'}^l f(\theta_{k_l}, \theta_{l_k}, R_{kl}) \left(\prod_{\neq k,l}^N \delta_{j_n j_n'} \right) \quad (3)$$

where $f(\theta_{k_l}, \theta_{l_k}, R_{kl})$ is

$$f(\theta_{k_l}, \theta_{l_k}, R_{kl}) \equiv \left(\cos(\theta_{k_l} - \theta_{l_k}) - 3 \cos\theta_{k_l} \cos\theta_{l_k} \right) / \left(4\pi\varepsilon_0 R_{kl}^3 \right). \quad (4)$$

By diagonalizing the Hamiltonian matrix H [Eq. (1)], we can obtain eigenenergies $\{E_l^{\text{agg}}\}$ and eigenstates $\{|\psi_l^{\text{agg}}\rangle\}$ $(l = 1, \ldots, M)$, where M is the size of the basis used. The M is $1 + {}_N\text{C}_1 + {}_N\text{C}_2$ since we consider one and two excitons, which are at least necessary for describing the third-order nonlinear optical processes. The transition dipole matrix element $(\mu_{ll'}^{\text{agg}})$ in the direction of the applied field for this new state model is also calculated by

$$\mu_{ll'}^{\text{agg}} \equiv \langle \psi_l^{\text{agg}} | \mu^{\text{agg}} | \psi_{l'}^{\text{agg}} \rangle = \sum_{\substack{j_1,\ldots,j_N \\ j_1',\ldots,j_N'}} \langle \psi_l^{\text{agg}} | \varphi_{j_1}^1 \cdots \varphi_{j_N}^N \rangle \times \langle \varphi_{j_1'}^1 \cdots \varphi_{j_N'}^N | \psi_{l'}^{\text{agg}} \rangle \sum_k^N \mu_{j_k j_k'}^k \left(\prod_{n \neq k}^N \delta_{j_n j_n'} \right) \quad (5)$$

where $\mu_{j_k j_k'}^{\prime k}$ represents a transition dipole matrix element (in the direction of the polarization vector of the applied field) between j_k and j_k' of monomer k. It is noted that the transition moments between the ground and one-exciton states, and those between one- and two-exciton states, exist in the present model.

DENSITY MATRIX FORMALISM FOR A MOLECULAR AGGREGATE INTERACTING WITH TIME-DEPENDENT ELECTRIC FIELDS

The time evolution of a molecular aggregate model is described by the following density matrix formalism [15]:

$$i\hbar \frac{\partial}{\partial t} \rho(t) = \left[H(t), \rho(t) \right] - i\Gamma\rho(t) \quad (6)$$

where $\rho(t)$ indicates the total molecular density matrix, and the second term on the right-hand side of Eq. (6) represents the relaxation processes in the Markov approximation. The total Hamiltonian $H(t)$ is expressed by the sum of the aggregate Hamil-

tonian H_{agg} and the aggregate-field interaction $V(t)$:

$$H(t) = H_{\rm agg} + V(t) = \sum_{l=1}^{M} E_l^{\rm agg} b_l^+ b_l - \sum_{l,l'=1}^{M} \mu_{ll'}^{\rm agg} (3F\cos\omega t) b_l^+ b_{l'} \quad (7)$$

where F is an external field amplitude in the direction of x since the incident field is assumed to be a plane wave with frequency ω and wave vector $\mathbf{k}$ traveling perpendicular to the molecular plane and the polarization vector is parallel to the x axis. The b_l^+ and b_l represent, respectively, the creation and annihilation operators for the l state of the aggregate state model obtained in the previous section. It is noted that the present incident field is $3F\cos\omega t$ since we consider the case of third-order harmonic generation (THG). The matrix representation of Eq. (7) is expressed as

$$\rho_{ll'}(t) = -i(1-\delta_{ll'})E_{ll'}^{\rm agg}\rho_{ll'}(t) - i\sum_{m}^{M}\big(V_{lm}(t)\rho_{ml'}(t) - \rho_{lm}(t)V_{ml'}(t)\big) - \big(\Gamma\rho(t)\big)_{ll'} \quad (8)$$

where $V_{ll'}(t) = -\mu_{ll'}^{\rm agg}(3F\cos\omega t)$.

The relaxation term $(-(\Gamma\rho(t))_{ll'})$ in Eq. (8) can be considered as the following two types of mechanisms [15]:

$$-\big(\Gamma\rho(t)\big)_{ll} = -\Gamma_{ll}\rho_{ll}(t) + \sum_{m\neq l}^{M}\gamma_{ml}\rho_{mm}(t) \quad (9)$$

and

$$-\big(\Gamma\rho(t)\big)_{ll'} = -\Gamma_{ll'}\rho_{ll'}(t). \quad (10)$$

Equations (9) and (10) describe the population and coherent-damping mechanisms, respectively. The $\gamma_{ll'}(\neq\gamma_{l'l})$ represents a feeding parameter. The off-diagonal damping parameter is expressed as

$$\Gamma_{ll'} = \tfrac{1}{2}(\Gamma_{ll} + \Gamma_{l'l'}) + \Gamma'_{ll'} \quad (11)$$

and

$$\Gamma_{ll'} = \Gamma_{l'l} \quad (12)$$

where $\Gamma'_{ll'}$ is the pure dephasing factor. In this study, since we assume a closed system, the factor γ_{li} is related to the decay rate as

$$\Gamma_{ll} = \sum_{i\neq l}^{M}\gamma_{li} \quad (13)$$

We perform a numerically exact calculation to solve Eq. (8) by the fourth-order Runge–Kutta method. The density matrix representation in the aggregate basis $\{|\varphi_{i_1}^1\varphi_{i_2}^2\cdots\varphi_{i_N}^N\rangle\}$ at time t is calculated by

$$\rho_{i_1,i_2,\ldots,i_N;i'_1,i'_2,\ldots,i'_N} = \sum_{l,l'=1}^{M}\big\langle\varphi_{j_1}^1\cdots\varphi_{i_N}^N\big|\psi_l^{\rm agg}\big\rangle \times\rho_{ll'}(t)\big\langle\psi_{l'}^{\rm agg}\big|\varphi_{j'_1}^1\cdots\varphi_{j'_N}^N\big\rangle \quad (14)$$

where $\rho_{ll'}(t)$ is calculated by Eq. (8). Using this density matrix, the polarization $p(t)$ is calculated by

$$p(t) = \sum_{\substack{i_1,i_2,\ldots,i_N\\ i'_1,i'_2,\ldots,i'_N}}^{M}\mu_{i_1,i_2,\ldots,i_N;\,i'_1,i'_2,\ldots,i'_N}\rho_{i'_1,i'_2,\ldots,i'_N;\,i_1,i_2,\ldots,i_N}(t). \quad (15)$$

Here, the transition matrix element $\mu_{i_1,i_2,\ldots,i_N;\,i'_1,i'_2,\ldots,i'_N}$ is represented by

$$\mu_{i_1,i_2,\ldots,i_N;\,i'_1,i'_2,\ldots,i'_N} = \left\langle\varphi_{i_1}^1\cdots\varphi_{i_N}^N\middle|\sum_{l=1}^{N}\mu^{\prime l}\middle|\varphi_{i'_1}^1\cdots\varphi_{i'_N}^N\right\rangle = \sum_{i=1}^{N}\mu_{i_l i'_l}^{\prime l}\left(\prod_{n\neq l}^{N}\delta_{i_n i'_n}\right) \quad (16)$$

where $\mu_{i_l i'_l}^{\prime l}$ represents a transition dipole matrix element (in the direction of the polarization vector of the applied field) between i_l and i'_l of monomer l.

NONPERTURBATIVE SECOND HYPERPOLARIZABILITY AND ITS PARTITION INTO THE CONTRIBUTION OF EXCITON GENERATION

We briefly explain our definition and a calculation method of nonperturbative γ [15] in THG. The polarization ($p(t)$) is transformed to $p(\omega)$ in the frequency domain by using the following discrete Fourier transformation:

$$p(\omega_j) = \frac{1}{n}\sum_{k=0}^{n-1}p(t_k)\exp\left[i\left(\frac{2\pi}{n}jk\right)\right], \quad j = 0,1,\ldots,n-1;\ k = 0,1,\ldots n-1. \quad (17)$$

Here, the used number of time-series data is n, the nth discrete time is $t_k = (L/n)k$, and the jth discrete frequency is $\omega_j = (2\pi/L)_j$, where the minimum t value (t_0) is 0 and the maximum t value (t_{n-1}) is L. Using the external field amplitude $\varepsilon(\omega)(=F/2)$ and the polarization $p(\omega)$, the nonperturbative $\gamma(-3\omega;\omega,\omega,\omega)$ for a molecular aggregate is defined by

$$\gamma(-3\omega;\omega,\omega,\omega) = \frac{p(3\omega)}{27\varepsilon^3(\omega)}. \quad (18)$$

For weak fields, this quantity coincides with the conventional perturbative $\gamma(-3\omega;\omega,\omega,\omega)$. In contrast, for intense external fields, this quantity can exhibit various intensity-dependent phenomena [15]. Using Eqs. (15) and (16), the $\gamma(-3\omega;\omega,\omega,\omega)$ is also expressed as

$$\gamma(-3\omega;\omega,\omega,\omega) = \sum_{a>b}^{M} \gamma_{a-b} = \sum_{a>b}^{M} \frac{2\mu_{ab}\rho_{ba}^{\mathrm{real}}(3\omega)}{27\varepsilon^3(\omega)} \quad (19)$$

where a and b indicate the aggregate basis $\{|\varphi_{i_1}^1 \cdots \varphi_{i_N}^N|\}$, and $\rho_{ba}^{\mathrm{real}}$ is a real part of density matrix element in the aggregate basis. Equation (19) indicates that the total γ can be partitioned into the virtual excitation contribution (γ_{a-b}) between bases a and b. In the two-exciton model, the μ_{ab} exists between the $|11\cdots1\rangle$ (1: the ground state of the monomer) and one-exciton states, e.g., $|121\cdots1\rangle$ (2: the excited state of the monomer), or between one- and two-exciton states, so that the γ_{a-b} represents the contribution to γ of the virtual one- or two-exciton generation represented by a basis pair a–b. We can elucidate the spatial contribution of γ_{a-b} by showing exciton distribution represented by bases a and b. In this study, we represent the spatial contributions of one- and two-exciton generations to γ by summing up the γ_{a-b} concerning one- or two-exciton basis a (b) on each unit site.

Results and Discussion

TWO TYPES OF DENDRITIC AGGREGATES WITH AND WITHOUT A FRACTAL STRUCTURE

We consider two types of dendritic molecular aggregates with different sizes (*D*9 and *D*24) shown in Figure 1. They involve all of the same dipole units. The excitation energy and transition moment of the dipole unit (monomer) are assumed to be 38,000 cm^{-1} and 5 D, respectively. *D*9 has a nonfractal structure in the sense that the numbers of dipole units involved in regions **e** and **a**, which belong to adjacent different generations, respectively, are equal to each other. In contrast, *D*24 has a fractal structure since the number of dipole units involved in region **a**′ is larger than that in region **e**′. The one- and two-exciton states for these dendritic aggregates are shown in Figure 2. Both one- and two-exciton states are found to have multistep energy structures, which are distributed around E_{21} (the excitation energy of the monomer) and $2E_{21}$, respectively. Such multistep energy structures can be explained by the *J*- and *H*-aggregate-type interactions [17, 18] involved in the dendritic structure. Apparently, the widths of the multistep energy states for *D*24 are larger than those for *D*9. This indicates that the number of intermolecular interaction pairs in *D*24 is larger than that in *D*9. The relaxation factor

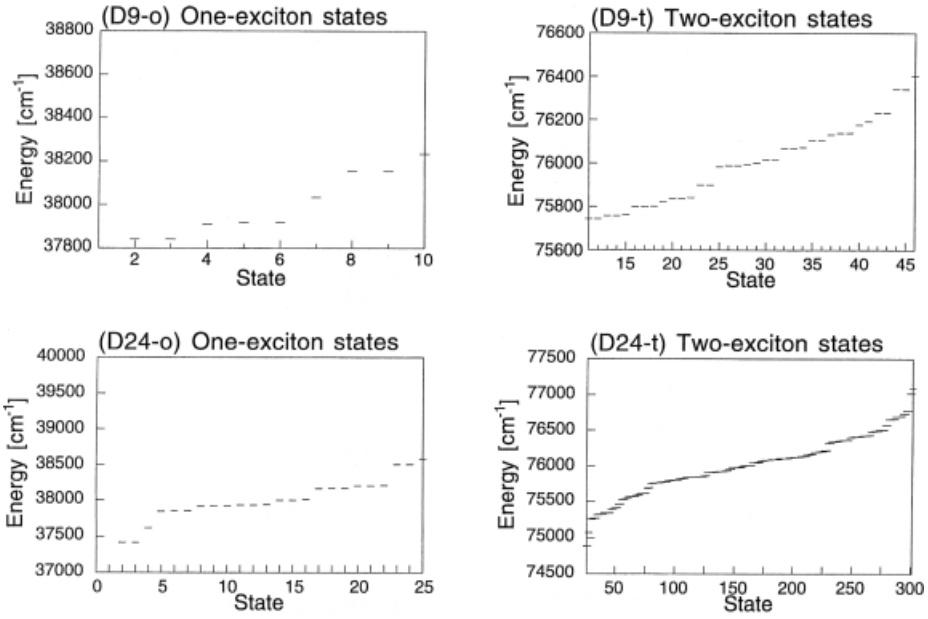

FIGURE 2. Calculated one- and two-exciton states for *D*9 [(*D*9-*o*) and (*D*-9-*t*)] and for *D*24 [(*D*24-*o*) and (*D*24-*t*)].

γ_{li} in Eq. (13) is determined by an energy-dependent relation: $\gamma_{li} = f(E_l^{\rm agg} - E_i^{\rm agg})$ ($f = 0.02$, $l(> i)$: one- or two-exciton state). This indicates that the population of the higher one(two)-exciton state decreases faster, and damps into the lower one(two)-exciton states. Such relaxation in exciton states is found to be essential for the exciton migration from the periphery to the core in these dendritic systems [13]. The external single-mode laser with 10 MW/cm^2 has a frequency of 3000 cm^{-1}, which is sufficiently off-resonant with respect to exciton states. The division number of the one optical cycle of the external field used in the numerical calculation is 100, and the γ is calculated by using 20 optical cycles after an initial nonstationary time evolution (300 cycles).

Before investigating γ for these systems, we briefly explain the virtual excitation process of the third-order nonlinear optical phenomena. The γ is described by the following perturbational formula [15]:

$$\gamma = \gamma^{(\rm I)} = \gamma^{(\rm II)} + \gamma^{(\rm III)} = \sum_{n=2} \frac{(\mu_{n1})^2(\mu_{nn})^2}{E_{n1}^3} - \sum_{n=2} \frac{(\mu_{n1})^4}{E_{n1}^3} + \sum_{\substack{m,n=2 \\ (m\neq n)}} \frac{(\mu_{n1})^2(\mu_{mn})^2}{E_{n1}^2 E_{m1}}. \quad (20)$$

Here, μ_{n1} is the transition moment between the ground (1) and the nth excited states, μ_{mn} is the transition moment between the mth and the nth excited states, μ_{nn} is the difference of dipole moments between the ground and the nth excited states, and E_{n1} is the transition energy given by $(E_n - E_1)$. From these equations, apparently, the contributions of types I and III are positive in sign, whereas the contribution of type II is negative. It is noted that the type I contribution of the present dendritic aggregate vanishes since the dipole moments of the ground and excited states for the dendritic aggregate are zero.

SPATIAL CONTRIBUTIONS OF ONE- AND TWO-EXCITON GENERATIONS TO γ OF *D*9

In this section, we elucidate the exciton contribution to γ of a dendritic aggregate (*D*9) with a nonfractal structure. From Eq. (20), types II and III virtual excitation contributions are found to be more enhanced in the case of smaller transition energies and larger magnitudes of transition moment. Figure 3 shows the sum of partitioned γ_{a-b} on each site for *D*9, including intermolecular interaction and relaxation effects. It is found that the main contributions of total, one-exciton, and two-exciton contributions are distributed in leg regions **a**, **h**, and **i**. This feature can be understood by the fact that these regions possess dominant interaction with the applied field since their dipole units are parallel to the polarization vector of the applied field. Each exciton contribution (one-exciton contribution $= -141,330$ a.u., two-exciton contribution $=$ 99,000 a.u.) is found to have a mutually opposite sign, and to have a much larger magnitude than the total γ ($-42,330$ a.u.). The one-exciton contribution (corresponding to type I) is found to be larger than the two-exciton contribution (corresponding to type II), so that the total γ value is found to be negative in sign. This feature reflects the fact that the present dendritic aggregate is composed of two-state monomers which provide only a type II (negative) contribution. Namely, in the present

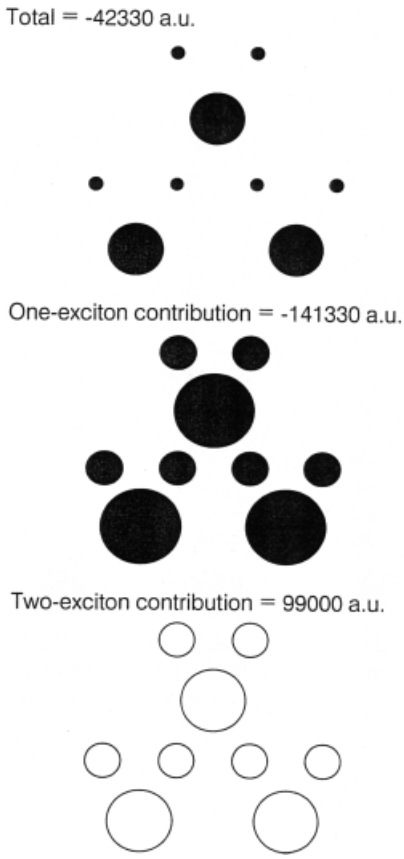

FIGURE 3. Calculated γ ($= \gamma_{xxxx}$) [a.u.] and the one- and two-exciton contributions (spatial contributions) of the dendritic aggregate *D*9 (Fig. 1) involving intermolecular interactions and relaxation effects. The size of the circle at each dipole site represents the magnitude of the contribution. This γ value is the same as $\gamma_{\rm int+rel}$ in Figure 4.

model, positive contribution (type III) originates in the two-exciton generation composed of excitations on two different sites.

EFFECTS OF INTERMOLECULAR INTERACTION AND RELAXATION ON THE SPATIAL CONTRIBUTIONS OF ONE- AND TWO-EXCITON GENERATIONS TO γ OF *D*9

Before discussing the effects of intermolecular interaction and relaxation, we define the notation of γ. The γ value, including only intermolecular-interaction effects, is referred to as γ_{int}, and the γ value including both intermolecular interaction and relaxation effects is referred to as $\gamma_{\text{int+rel}}$. The γ value including neither effect is referred to as γ_{non}.

First, we only focus on the effects of intermolecular interaction on γ, so that the relaxation terms are omitted. Figure 4(a) shows the effects of the intermolecular interaction on the one- and two-exciton generation contributions to γ. The total γ value is found to be slightly reduced by the intermolecular interaction compared to γ_{non} ($\gamma_{\text{int}} - \gamma_{\text{non}} = -761$ a.u.). The total γ value is found to be composed of the negative contribution of one-exciton generation (type II) and the positive contribution of two-exciton generation (type III). The primary contributions of one-exciton generation appear on sites **a**, **h**, and **i**, while their magnitudes are almost equal to each other. This feature originates in the configuration of dipoles parallel to the applied field. Namely, *J*-aggregate-type interaction effects, which enhance the magnitudes of one-exciton contributions to γ, are more enhanced in such regions. In contrast, the two-exciton contributions are shown to

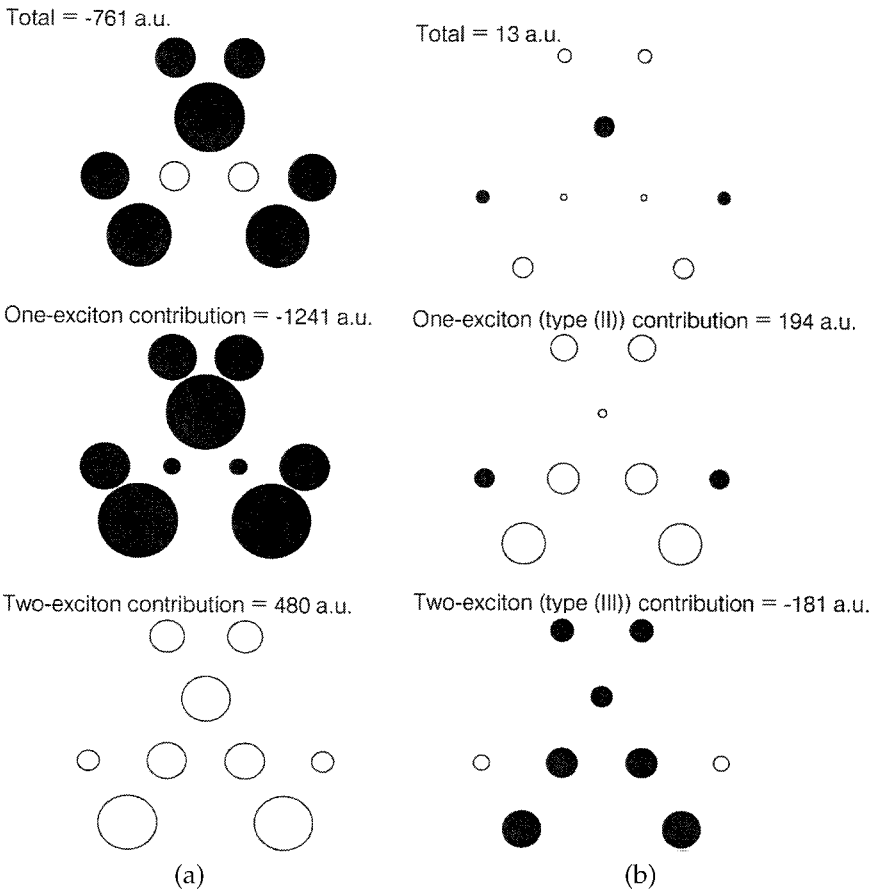

FIGURE 4. Difference ($\gamma_{\text{int}} - \gamma_{\text{non}}$) between exciton contributions to $\gamma (= \gamma_{xxxx})$ of *D*9 (Fig. 1) composed of interacting monomers and those composed of noninteracting monomers. Relaxation effects in exciton states are omitted in the case of (a). (b) Difference ($\gamma_{\text{int+rel}} - \gamma_{\text{int}}$) between exciton contributions to γ of *D*9 (Fig. 1) with relaxation effects and those without relaxation effects. (c) Total effects ($\gamma_{\text{int+rel}} - \gamma_{\text{non}}$) of intermolecular interaction and relaxation: (a) + (b). The white and black circles represent positive and negative contributions, respectively, and the size of the circle indicates the magnitude of contribution.

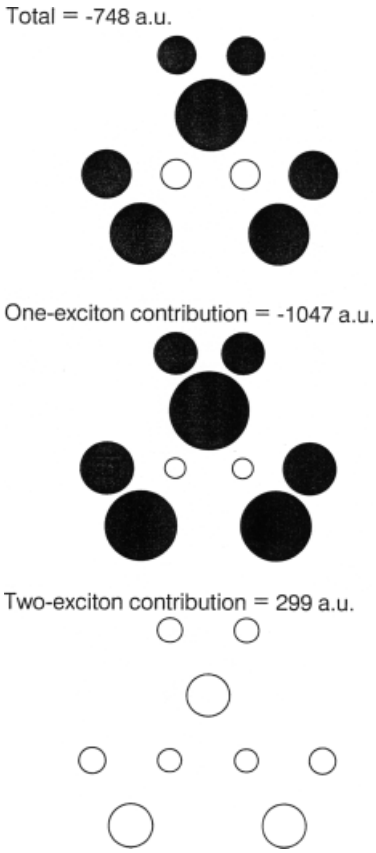

(c)

FIGURE 4. (Continued)

be distributed more extensively in the whole region of the aggregate compared to the one-exciton case. This feature reflects the fact that the two-exciton generation (on two different sites) occurs in a more spatially extensive region than the one-exciton generation (on a single site). In the present case, the one-exciton contribution is found to be larger than the two-exciton contribution. This is explained as follows. Although the *J*-aggregate-type intermolecular interaction decreases the exciton energies and then enhances one- and two-exciton contributions, the reduction of exciton energies contributes more to type II compared with type III in the present two-exciton models.

Next, we consider the relaxation effects in one- and two-exciton states on γ. It is found from Figure 4(b) that the relaxation effects slightly enhance the total γ compared to γ_{int} ($\gamma_{\mathrm{int+rel}} - \gamma_{\mathrm{int}} =$ 13 a.u.). The one- and two-exciton contributions are shown to be slightly reduced, respectively, and the degree of the variation is more remarkable on the periphery regions (**d**, **e**, **h**, and **i**). Judging from our way of introducing relaxation terms, these reductions are presumed to originate in the decoherence process, i.e., the decrease in the off-diagonal aggregate density matrices, due to the phase relaxation effects. Since the relaxation factor γ_{li} in Eq. (13) is determined by an energy-dependent relation, this reduction effect is expected to be more remarkable in higher exciton energy states (where the exciton is distributed on periphery regions). This feature corresponds to the relaxation effects on the spatial exciton contributions shown in Figure 4(b).

Although the intermolecular interaction and relaxation in one- and two-exciton states are found to provide effects with mutually opposite signs on γ, the total effects are found to slightly reduce γ in the *D*9 case [see Fig. 4(c)]. However, a larger relaxation factor or smaller intermolecular interaction could change the sign of the total effects on γ.

SPATIAL CONTRIBUTIONS OF ONE- AND TWO-EXCITON GENERATIONS TO γ OF *D*24

The spatial one-, two-, and total exciton contributions to off-resonant γ ($-135{,}050$ a.u.) of *D*24 (with a fractal structure) involving intermolecular interaction and relaxation effects are shown in Figure 5. All of the contributions of one-exciton generations are found to be negative in sign ($-930{,}570$ a.u.), while those of two-exciton generations are positive in sign (795,520 a.u.). In the present model, the one-exciton contribution is larger than the two-exciton contributions, so that the total γ value is negative in sign. It is found from Figure 5 that the main contributions are distributed in leg regions **j**′, **l**′, **n**′, **p**′, **i**′, **h**′, and **a**′. This feature can be understood by the fact that these regions possess dominant interaction with the applied field since their dipole units are parallel to the polarization vector of the applied field. Similar features are observed in the two-exciton contributions. The features of these spatial contributions in *D*24 (with a fractal structure) are equal to those in *D*9 (with a nonfractal structure).

EFFECTS OF INTERMOLECULAR INTERACTION AND RELAXATION ON THE SPATIAL CONTRIBUTIONS OF ONE- AND TWO-EXCITON GENERATIONS TO γ OF *D*24

Figure 6(a) shows the effects of the intermolecular interaction on the one- and two-exciton generation contributions to γ. The total γ value is found to be slightly reduced by the intermolecular interaction ($\gamma_{\mathrm{int}} = -23{,}968$ a.u.) since the one-exciton contributions ($-30{,}103$ a.u.) are found to much exceed

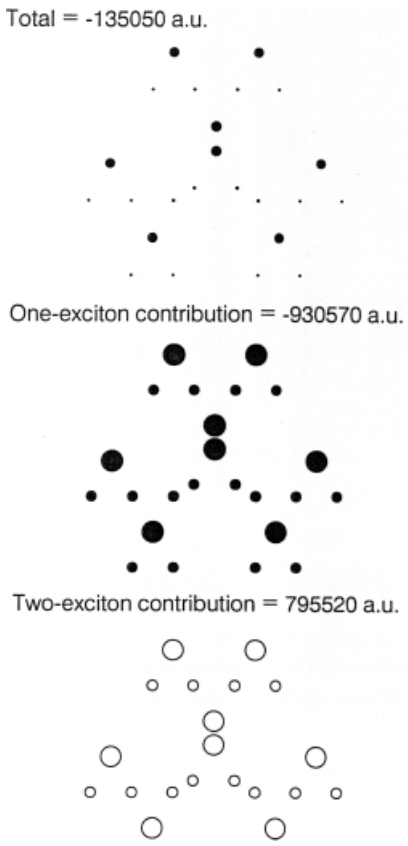

FIGURE 5. Calculated $\gamma (= \gamma_{xxxx})$ [a.u.] and the one- and two-exciton contributions (spatial contributions) for the dendritic aggregate *D*24 (Fig. 1) involving intermolecular interactions and relaxation effects. See Figure 3 for further legends.

(a)

FIGURE 6. (a) Difference $(\gamma_{\text{int}} - \gamma_{\text{non}})$ between exciton contributions to $\gamma (= \gamma_{xxxx})$ of *D*24 (Fig. 1) composed of interacting monomers and those composed of noninteracting monomers. Relaxation effects in exciton states are omitted in the case of (a). (b) Difference $(\gamma_{\text{int+rel}} - \gamma_{\text{int}})$ between exciton contributions to γ of *D*24 (Fig. 1) with relaxation effects and those without relaxation effects. (c) Total effects $(\gamma_{\text{int+rel}} - \gamma_{\text{non}})$ of intermolecular interaction and relaxation: (a) + (b). See Figure 4 for further legends.

the two-exciton contributions (6135 a.u.). Similarly to the *D*9 case, the enhancement of the magnitudes of one- and two-exciton contributions is ascribed to the reduction of excitation energies caused by the *J*-aggregate-type intermolecular interaction in linear leg regions $\mathbf{j}'$, $\mathbf{l}'$, $\mathbf{n}'$, $\mathbf{p}'$, $\mathbf{i}'$, $\mathbf{h}'$, and $\mathbf{a}'$. The relative magnitudes of one- and two-exciton contributions are determined by the relative magnitudes of types II and III contributions [Eq. (20)]. In contrast to the *D*9 case, the contributions are put in the magnitude order: ($\mathbf{a}'$), ($\mathbf{h}'$ and $\mathbf{i}'$), and ($\mathbf{l}'$, $\mathbf{j}'$, $\mathbf{p}'$, and $\mathbf{n}'$). This implies that the quantum coherency between the exciton and the ground states is more enhanced in more internal linear legs parallel to the polarization vector of the applied field. This feature can be explained by the larger interaction of dipoles in such regions with the applied field, and the significant decrease in the exciton energies due to the larger *J*-aggregate-type interactions in going from the periphery to the core. We can conclude that this increase in the spatial contribution of exciton generation from the periphery to the core originates in the fractal structure of *D*24.

Next, we consider the relaxation effects in one- and two-exciton states on γ. It is found from Figure 6(b) that the relaxation effects very slightly reduce the total $\gamma (\gamma_{\text{int+rel}} - \gamma_{\text{int}} = -4.9155$ a.u.). The one- and two-exciton contributions are found to slightly decrease the magnitudes of those contributions, respectively. The dominant reductions occur in regions $\mathbf{j}'$, $\mathbf{l}'$, $\mathbf{n}'$, $\mathbf{p}'$,$\mathbf{i}'$, $\mathbf{h}'$, and $\mathbf{a}'$ and their magnitudes slightly decrease in going from the periphery to the core. This feature is caused by the fact that

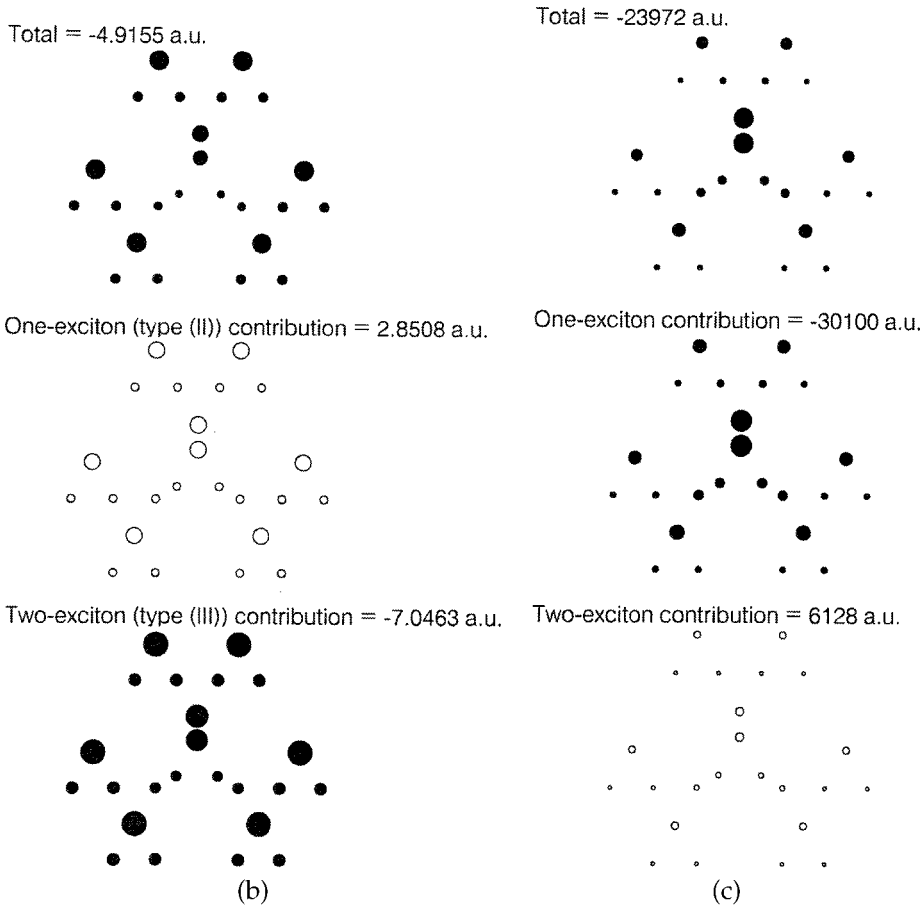

FIGURE 6. (Continued)

the decoherence process is more remarkable in the periphery regions (higher energy exciton states). It is also found that the magnitudes of the relaxation effects on one- and two-exciton contributions to γ for *D*24 are much smaller than those for *D*9. This feature seems to be related to the fact that the feeding population to the lower exciton states somewhat causes the decrease in the decoherence. Namely, it is probable that, since *D*24 has a larger number of lower exciton states than *D*9, these effects become large in *D*24, and then significantly reduce the reduction effects of γ by the relaxation.

Although the intermolecular interaction and relaxation in the one(two)-exciton state are found to provide effects with mutually opposite signs on γ, both the intermolecular interaction and relaxation effects are found to slightly reduce γ in the present case [see Fig. 6(c)]. However, this change in sign and magnitudes depends on the relative magnitudes between the relaxation factor and the strength of the intermolecular interaction.

Conclusions

In this study, we investigated the effects of intermolecular interaction and relaxation on the one- and two-exciton contributions to γ for two different sizes of dendritic molecular aggregates, *D*9 (with a nonfractal structure) and *D*24 (with a fractal structure), by visualizing the spatial contributions of exciton generations to off-resonant γ. These aggregates are found to provide negative γ, which are composed of the negative contribution of one-exciton generation and the positive contribution of two-exciton generation. The main contributions of one- and two-exciton generations are found to be distributed in the linear leg regions parallel to the polarization vector of the applied field since the interactions among their dipole units and the applied field are larger than others. It is also noted that there is a distinct difference in the intermolecular-interaction effects

on the spatial contribution of exciton generation between fractal and nonfractal structures: for *D*9 (with a nonfractal structure), the contributions of exciton generations distributed on such leg regions are found to be almost equal to each other, while for *D*24 (with a fractal structure), those are found to be more enhanced in going from the periphery to the core since more internal regions have more *J*-aggregate-type-interaction pairs, which lead to more of a decrease in exciton energies, and thus enhance the contribution to γ more. In contrast, the relaxation in the one- and two-exciton states is found to decrease their contributions, especially in the periphery regions. This is ascribed to the decoherence of off-diagonal aggregate density matrices between the ground and higher exciton states (mainly distributed on the periphery regions) caused by the relaxation effects. However, the enlargement of the size of aggregates seems to reduce the decrease in the contributions since lower exciton states (distributed in the internal regions) gain population fed by higher exciton states. In conclusion, larger size fractal dendritic aggregates composed of two-state monomers are expected to cause a more remarkable enhancement of the contribution from the periphery to the core due to the larger number of *J*-aggregate-type-interaction pairs in internal generations. Although, in the present case, the total $|\gamma|$ is finally found to be enhanced by including these two effects, the reduction of $|\gamma|$ can be observed under other conditions, e.g., larger relaxation factors and smaller intermolecular interactions. Further, dendritic aggregates composed of three-state monomers have the possibility of exhibiting positive total γ since the type III (positive) contribution exists even in a monomer. The investigation of the contributions of exciton generations to γ for such systems is in progress in our laboratory.

ACKNOWLEDGMENTS

This work was supported by Grant-in-Aid for Scientific Research on Priority Areas (Nos. 10185101, 12042248, and 12740320) from the Ministry of Education, Science, Sports and Culture, Japan.

References

1. Knox, R. S. Primary Processes of Photosynthesis; Barber, J., Ed.; Elsevier: Amsterdam, The Netherlands, 1977; p. 55.
2. Pope, M.; Swenberg, C. E. Electronic Processes in Organic Crystals; Oxford University Press: Oxford, England, 1982.
3. Webber, S. E. Chem Rev 1990, 90, 1469.
4. Tomalia, D. A.; Naylor, A. M.; Goddard, W. A. Angew Chem Int Ed Engl 1990, 29, 138.
5. Jiang, D.-L.; Aida, T. Nature 1997, 388, 454.
6. Mukamel, S. Nature 1997, 388, 425.
7. Fox, M. A.; Jones, W. E.; Watkins, D. M. Chem Eng News 1993, 119, 6197.
8. Devadoss, C.; Bharathi, P.; Moore, J. S. J Am Chem Soc 1996, 118, 9635.
9. Shortreed, M. R.; Swallen, S. F.; Shi, Z.-Y.; Tan, W.; Xu, Z.; Devadoss, C.; Moore, J. S.; Kopelman, R. J Phys Chem B 1997, 101, 6318.
10. Kopelman, R.; Shortreed, M.; Shi, Z.-Y.; Tan, W.; Bar-Haim, A.; Klafter, J. Phys Rev Lett 1997, 78, 1239.
11. Bar-Haim, A.; Klafter, J.; Kopelman, R.; J Am Chem Soc 1997, 26, 6197.
12. Tretiak, S.; Chernyak, V.; Mukamel, S. J Phys Chem B 1998, 102, 3310.
13. Harigaya, H. Int J Mod Phys B 1999, 13, 2531; Phys Chem Chem Phys 1999, 1, 1687.
14. Nakano, M.; Takahata, M.; Fujita, H.; Kiribayashi, S.; Yamaguchi, K. Chem Phys Lett, to appear.
15. Fujita, H.; Nakano, M.; Takahata, M.; Kiribayashi, S.; Nagao, H.; Yamaguchi, K. Nonlinear Opt, to appear.
16. Nakano, M.; Yamaguchi, K. Phys Rev A 1994, 50, 2989.
17. Spano, F. C.; Knoester, J. Adv Magn Opt Res 1994, 18, 117.
18. Spano, F. C.; Kuklinski, J. R.; Mukamel, S. Phys Rev Lett 1990, 65, 211.